

THE DEPENDENCE OF BROWN DWARF RADII ON ATMOSPHERIC METALLICITY AND CLOUDS: THEORY AND COMPARISON WITH OBSERVATIONS

ADAM BURROWS¹, KEVIN HENG², AND THANE NAMPAISARN¹

Accepted to Ap.J. May 3, 2011

ABSTRACT

Employing realistic and consistent atmosphere boundary conditions, we have generated evolutionary models for brown dwarfs and very-low-mass stars (VLMs) for different atmospheric metallicities ($[\text{Fe}/\text{H}]$), with and without clouds. We find that the spread in radius at a given mass and age can be as large as $\sim 10\%$ to $\sim 25\%$, with higher-metallicity, higher-cloud-thickness atmospheres resulting quite naturally in larger radii. For each 0.1 dex increase in $[\text{Fe}/\text{H}]$, radii increase by $\sim 1\%$ to $\sim 2.5\%$, depending upon age and mass. We also find that, while for smaller masses and older ages brown dwarf radii decrease with increasing helium fraction (Y) (as expected), for more massive brown dwarfs and a wide range of ages they increase with helium fraction. The increase in radius in going from $Y = 0.25$ to $Y = 0.28$ can be as large as $\sim 0.025 R_{\text{J}}$ ($\sim 2.5\%$). Furthermore, we find that for VLMs an increase in atmospheric metallicity from 0.0 to 0.5 dex, increases radii by $\sim 4\%$, and from -0.5 to 0.5 dex by $\sim 10\%$. Therefore, we suggest that opacity due to higher metallicity might naturally account for the apparent radius anomalies in some eclipsing VLM systems. Ten to twenty-five percent variations in radius exceed errors stemming from uncertainties in the equation of state alone. This serves to emphasize that transit and eclipse measurements of brown dwarf radii constrain numerous effects collectively, importantly including the atmosphere and condensate cloud models, and not just the equation of state. At all times, one is testing a multi-parameter theory, and not a universal radius–mass relation.

Subject headings: stars: brown dwarfs

1. INTRODUCTION

For the last fifteen years, the evolutionary, spectral, and atmospheric theory of brown dwarfs has evolved in tandem with the explosive growth in the number of known examples. That number now stands near 1000. This maturing theory has been used to interpret spectroscopic and photometric observations of such substellar-mass objects (SMOs) and, thereby, to derive effective temperatures (T_{eff}), gravities (g), bolometric luminosities, compositions, masses (M), and ages (t). The focus of study has been the new spectroscopic types, L and T, that have emerged to accommodate objects with T_{eff} s from ~ 500 K to ~ 2200 K. Both chemical equilibrium and non-equilibrium models have found roles and gradual improvements in molecular opacity and thermochemical databases suggest that objects with molecular atmospheres may someday be studied with the same precision as are stars with simpler atomic atmospheres, the latter albeit after almost a century of development.

However, most brown dwarfs are found as singletons, and those in binaries have only rarely been used to derive dynamical masses with which to provide independent checks on spectroscopically-derived masses (Konopacki et al. 2010; Liu, Dupuy, & Leggett 2010). Too often, however, such comparisons are cast as fundamental tests of core assumptions in the models. Little mention is made of the equal importance of atmospheric

opacities, metallicities, cloud models, and ages in determining whether theory fits data. In fact, these last-mentioned quantities are crucial in determining the physical properties of a given brown dwarf.

In addition to obtaining independent masses, measuring the radii of brown dwarfs can be an equally powerful means of testing the associated physical theory (Burgasser, Burrows, & Kirkpatrick 2006). However, here too one is testing a multi-parameter theory, and not a universal radius (R)–mass relation. The latter exists only for cold, very old, objects of a given elemental composition. Hot, evolving brown dwarfs with a priori unknown atmospheric and interior compositions (and opacities) can span a (wide) range (perhaps 25%) of radii for a given mass and age. The brown dwarf’s atmospheric opacities determine the rate with which heat escapes the convective core, and at which the core entropy evolves, and it is the core entropy which sets the radius, for a given mass and internal composition.

Gas-phase atmospheric opacities can be augmented by silicate and iron cloud opacities. The presence of clouds, for which there is as yet no rigorous or credible model, complicates the theory and interpretation of the measured physical properties of brown dwarfs. The thicker the atmosphere, the slower the radius shrinks and the larger is the radius at a given mass and age. Since the gas-phase opacities depend upon composition (atmospheric metallicity) and extant cloud models are still crude, without additional constraints on these factors there is an inherent ambiguity in the comparison between measured and theoretical radii that should temper any conclusions drawn. What is more, rapid rotation and (perhaps) magnetic activity (Chabrier, Gallardo, & Baraffe 2007; Morales et al. 2009) can further compli-

¹Department of Astrophysical Sciences, Peyton Hall, Princeton University, Princeton, NJ 08544; burrows@astro.princeton.edu, tnampais@astro.princeton.edu

²Institute for Advanced Study, School of Natural Sciences, 1 Einstein Drive, Princeton, NJ 08540, U.S.A.; ETH Zurich, Institute for Astronomy, Wolfgang-Pauli-Strasse 27, CH-8093, Zurich, Switzerland; kheng@phys.ethz.ch

cate the interpretation of an observed radius and what one can deduce from differences between measured and model radii.

For a given mass and age there is a physical, realistic *range* of possible radii that varies with atmospheric metallicity and cloud optical depth, both of which would need to be measured to properly falsify theoretical models. For simplicity, evolutionary models have frequently been provided by theorists for only a restricted set of parameters (e.g., at solar metallicity) and for a single ad hoc prescription for clouds (or with no clouds) (Burrows et al. 1993,1997,2001,2006; Chabrier & Baraffe 1997; Baraffe et al. 1998,2003; Saumon & Marley 2008). However, these models have been applied quite generally, with an assumption of universality that is not warranted. As a consequence, any deviation between these theoretical models and physical measurements, be they of radius or mass, must first account for the effects of different atmospheres before declaring anything about, for example, the underlying equation of state or fundamental assumptions of the modeling exercise. Moreover, without a good constraint on the age of the brown dwarf (perhaps from a good estimate of the primary’s age and the assumption of coevality), any radius measurement is of correspondingly limited utility if the goal is to test structural theory beyond its “zeroth-order” aspects.

Recently, numerous exoplanet transit surveys have collectively discovered and characterized more than one hundred transiting companions to nearby stars. These surveys include *Kepler* (Koch et al. 2010; Borucki et al. 2010), *CoRoT* (Baglin et al. 2006), WASP (Pollacco et al. 2004), OGLE (Udalski et al. 2002; Konacki et al. 2003), and HAT (Bakos et al. 2002). Importantly, byproducts of such surveys, and their radial-velocity follow-up, are radii and masses for almost all of them, enabling the type of structural study to which we alluded above. Most of the transiting companions have masses near or below that of Jupiter and most of them are very close to their primaries. Such proximity introduces the need to incorporate the effects of irradiation (and perhaps tidal heating) in any interpretative study of the radius–mass relation of objects in this mass range. However, a small subset of the transiting companions found are quite massive (above $\sim 15 M_J$) and the radii of such SMOs should not be affected by stellar irradiation (Burrows et al. 2007). Therefore, data for these more massive objects can be used to constrain brown dwarf theory. Of most interest for such a study are *Kepler*’s LHS 6343 (Johnson et al. 2010), CoRoT-15b (Bouchy et al. 2011), CoRoT-3b (Deleuil et al. 2008), and WASP-30b (Anderson et al. 2011). Since they reside in a physical region that is seamlessly connected to that of brown dwarfs, the very-low-mass stars (VLMs) OGLE-TR-122b (Pont et al. 2005) and OGLE-TR-123b (Pont et al. 2006), though of stellar mass, test the same basic theories.

In this paper, we calculate a new suite of evolutionary models with new sets of atmospheric boundary conditions for various atmospheric metallicities, with and without clouds (i.e., clear). With these models, we are able to demonstrate and quantify the dependence of the radius of a brown dwarf of a given mass and age on the variety of different atmospheric characteristics expected. Brown dwarfs should vary in metallicity and

cloud cover. Higher-metallicity atmospheres cool more slowly and, therefore, result in larger brown dwarf radii, all else being equal. Cloudy atmospheres similarly retard radius shrinkage and lead to larger radii at a given mass and age. Though we do not yet know how to incorporate this possibility, higher-metallicity atmospheres may also have thicker cloud decks, amplifying the effect of increasing metallicity. Be that as it may, one should expect a range of realistic brown dwarf radii at a given mass and age. Our paper quantifies this range to highlight this important fact, while also exploring the dependence on the helium mass fraction (Y).

With the models we generate, we fit various of the recently measured transiting brown dwarf radii. We have chosen for this study the brown dwarfs LHS 6343C (Johnson et al. 2010), CoRoT-15b (Bouchy et al. 2011), CoRoT-3b (Deleuil et al. 2008), and WASP-30b (Anderson et al. 2011), and the VLMs OGLE-TR-122b (Pont et al. 2005) and OGLE-TR-123b (Pont et al. 2006), but the generic nature of the expected spread in radius at a given mass and age is the true focus of this investigation.

While documenting representative theoretical differences in radius evolutions for different metallicities and helium fractions (with and without clouds), we at the same time demonstrate that radius–mass measurements do not constrain solely the equation of state. The atmospheric opacities (and, less so, the helium fraction and overall internal compositions) are important factors in the interpretation of any radius measurement. Moreover, the significant remaining uncertainties in the ages of all these systems, and the difficulties and potential systematic inaccuracies in the measurements themselves, partially undermine any attempt to arrive at definitive conclusions concerning the accuracy or usefulness of any theoretical evolutionary model. Nevertheless, the magnitude of the expected theoretical spread in radii for brown dwarfs at a given mass and age should be more robust, and, as we demonstrate, is certainly not trivial.

In section 2, we summarize the data for the transiting objects upon which we focus in this paper. Then, in section 3 we review the techniques we have employed to calculate the evolutionary models, using an atmosphere/spectral code to obtain the boundary conditions for our Henyey evolutionary code. In section 4, we discuss the general trends and behaviors of the full model suite, after which in section 5 we determine individual object characteristics from comparisons with the collection of new models. Finally, in section 6, we review the overarching conclusions concerning the radius–mass relation that have emerged from this study.

2. DATA SUMMARY

One of the most interesting objects in the observed set is LHS 6343C (Johnson et al. 2010), discovered using *Kepler*. It has a measured mass of $62.9 \pm 2.3 M_J$, a measured radius of 0.833 ± 0.021 , and orbits one of a pair of M dwarfs (LHS 6343A, with an inferred mass of $\sim 0.37 M_\odot$) with a period of 12.71 days. From the minimal chromospheric activity, the authors suggest an age greater than 1 Gyr (gigayear), and prefer a range of ~ 1 Gyr to ~ 5 Gyr. Anderson et al. (2011) quote a metallicity ($[Fe/H]$) for LHS 6343A of 0.28 ± 0.07 , but Johnson et al. (2010) provide a value of 0.04 ± 0.08 . The “triple” nature of this system complicated the extraction of phys-

ical parameters. We quote inferred metallicities for the primary of LHS 6343C (and for the other primaries discussed below) under the assumption that the primary and secondary metallicities of coeval objects formed in the same context are likely to be similar and that the primary’s [Fe/H] can serve as a guide when fitting secondary characteristics.

CoRoT-15b (Bouchy et al. 2011) has a measured mass of $63.3 \pm 4.1 M_J$, a measured radius of $1.12^{+0.30}_{-0.15} R_J$, and orbits its F7V star primary with a period of 3.06 days. Bouchy et al. (2011) suggest an age for CoRoT-15b of $\sim 1.14\text{--}3.35$ Gyr and a metallicity of $\sim 0.1 \pm 0.2$, basically solar. Deleuil et al. (2008) obtain a mass for CoRoT-3b of $21.66 \pm 1.0 M_J$ and a radius of $1.01 \pm 0.07 R_J$. These authors prefer an age and metallicity for the F3V primary CoRoT-3 of ~ 2 Gyr and -0.02 ± 0.06 , respectively, the latter consistent with solar. CoRoT-3b’s orbital period is 4.26 days.

WASP-30b (Anderson et al. 2011) has a measured mass of $60.96 \pm 0.89 M_J$ and a measured radius of $0.89 \pm 0.021 R_J$. Anderson et al. (2011) quote a metallicity for WASP-30 of -0.08 ± 0.10 , also basically solar, and prefer an age of 2.0 ± 1.0 Gyr. WASP-30b is orbiting its F8V primary with a period of 4.16 days.

The very-low-mass stars (VLMs) OGLE-TR-122b and OGLE-TR-123b have measured masses of $96 \pm 9 M_J$ (Pont et al. 2005) and $89 \pm 12 M_J$ (Pont et al. 2006), respectively. Their measured radii are $1.17^{+0.23}_{-0.13} R_J$ and $1.30 \pm 0.11 R_J$. Pont et al. (2005,2006) suggest that the ages of these VLMs are probably less than 0.5 Gyrs. The metallicity of OGLE-TR-122 is estimated to be 0.15 ± 0.36 , and, hence, can be considered unconstrained. OGLE-TR-122b is orbiting a solar-like star with a period of 7.3 days and OGLE-TR-123b is orbiting an F star with a period of 1.8 days. Both are at large distances (~ 1000 and ~ 1600 parsecs) and, hence, their primaries are difficult to characterize accurately. An interesting eclipsing system is 2MASS J0535 (Stassun et al. 2006), for which, curiously, the least massive of the pair has the higher measured T_{eff} . However, though its masses are both in the brown dwarf regime ($0.054 \pm 0.005 M_\odot$ and $0.034 \pm 0.003 M_\odot$) and the radii of these two objects are measured to be $0.669 \pm 0.034 R_\odot$ and $0.511 \pm 0.026 R_\odot$, respectively, the estimated system age is ~ 1 Megayear (Myr). At such young ages, one needs a theory for their formation in the context of the protostellar disk. Extant evolutionary models for isolated spherical objects that assumed the initial conditions were lost on timescales of tens of Myrs are not suitable for comparisons at Myr ages.

3. METHODOLOGY & ASSUMPTIONS

Our spectral and atmosphere methods have previously been described in Burrows et al. (1993,1997,2003,2006), but we repeat the salient points here for completeness. Given the surface gravity (g), effective temperature (T_{eff}) and cloud properties, the planar code COOLTLUSTY solves for the atmosphere and spectrum of an object using the hybrid technique of complete linearization and accelerated lambda iteration (Hubeny 1988; Hubeny & Lanz 1995), adopting the solution to the (gray) Milne problem as a first guess. Convection is treated using mixing length theory, where the mixing length L_{mix} in units

of the pressure scale height (H_p) is set to 1.0. Iteration proceeds until adjacent layers of the 1D atmosphere are in radiative equilibrium. We have computed cloud-free evolutionary tracks for $L_{\text{mix}} = 0.5H_p$, H_p and $2H_p$ and find that within the ranges of effective temperature ($T_{\text{eff}} = 200\text{--}3000$ K) and surface gravity ($\log_{10} g = 3.5\text{--}5.5$) considered in this paper, the models generated are essentially identical. The main gas-phase species used in these theoretical atmospheres are H_2 , He, H_2O , CO, CH_4 , N_2 , NH_3 , FeH, CrH, Na I, and K I and our spectral model employs 30000 frequency points from ~ 0.35 to 300 microns. The opacities are taken from Sharp & Burrows (2007).

To generate molecular abundances in chemical equilibrium at a given atmospheric metallicity, we employed the thermochemistry found in Sharp & Burrows (2007) and followed nearly 500 species (with over 150 condensates) containing 27 elements. For these abundance calculations, the atmospheric element fractions for a given metallicity were taken from Allende-Prieto, Lambert, & Asplund (2001), Asplund et al. (2005), and Allende-Prieto & Lambert (2005), which replaced the Anders & Grevesse (1989) compositions we used previously.

Refractory silicates condense out at temperatures below ~ 2300 K and above ~ 1700 K. In our chemical code, these species are rained out (Burrows & Sharp 1999) to determine the resulting gas-phase abundances. However, the clouds of the condensed refractories have a meteorology, physical extent, and particle-size distribution that are as yet unconstrained (Ackerman & Marley 2001; Helling et al. 2001,2004).

Therefore, to incorporate clouds into the spectral and atmosphere models, we introduce a flexible parametrization that allows us to vary cloud opacities and effects. For this study, we assume that the numerous cloud species are mimicked by one representative species (in this case forsterite, Mg_2SiO_4) that extends from a base at 2300 K to the intersection point of the atmospheric temperature-pressure profile with the forsterite ‘‘Clausius-Clapeyron’’ condensation line.

The baseline distribution of the cloud particle density is assumed to follow the gas-phase pressure profile, but we multiply this baseline reference distribution by a shape function, $f(P)$, to determine the actual model cloud distribution in pressure space. $f(P)$ is never greater than one and can be made to cut off sharply at the top and bottom of the cloud. Specifically, we define $f(P)$ as:

$$f(P) = \begin{cases} (P/P_u)^{s_u}, & P \leq P_u \\ f_{\text{cloud}}, & P_u \leq P \leq P_d \\ (P/P_d)^{-s_d}, & P \geq P_d, \end{cases} \quad (1)$$

where P_d is the pressure at the cloud base and $P_u < P_d$. Here, P_u is the pressure at the intersection of the atmospheric T/P profile and the forsterite condensation curve. The indices s_u and s_d define the rapidity with which the clouds are cut off on their upper and lower boundaries. The larger they are, the sharper the cutoff. When $f_{\text{cloud}} = 1$ the cloud has a flat portion in its middle between P_u and P_d . Hence, the parameters s_u , s_d , and f_{cloud} define the cloud spatial structure.

We chose ~ 2300 K as our cloud base since it is where the most refractory species (calcium-aluminum silicates)

condense. We chose the forsterite condensation line to cap this region because forsterite has one of the lowest condensation temperatures (for a given pressure). Hence, the physical region where refractory clouds reside is more extensive than where forsterite alone would reside. To attempt a multi-species meteorological model, incorporating the optical properties of all the expected refractories and the role of convection in grain growth, and to pretend to model the various particle sizes and shapes and the interaction between the various grain species (mantling, collisions, etc.), would introduce extra complexity wholly out of proportion with the sparse dataset available for these very-remotely-sensed objects.

Note that if only forsterite clouds obtained, the ‘‘Clausius-Clapeyron’’ condensation line would be the natural cloud base (and not the ~ 2300 K line), but that convection and turbulence would still likely extend the cloud upward to lower pressures. The characteristic scale of this is often assumed to scale with the pressure scale height. This is the motivation for introducing the parameter s_u , thereby capturing this physical extension above the forsterite condensation line.

For the cloud models in this study, we set $s_u = 2$ and $s_d = 10$ and use a modal particle size $a_0 = 30 \mu\text{m}$ (Sudarsky et al. 2000), where the size distribution is given by:

$$\frac{dN}{da} \propto \left(\frac{a}{a_0}\right)^6 \exp\left[-6\left(\frac{a}{a_0}\right)\right]. \quad (2)$$

We use Mie scattering theory with a table of complex indices of refraction as a function of wavelength to calculate the absorption and scattering opacities for the grains in the clouds. In summary, with this general cloud model we place clouds where they may be likely to reside, over the collective condensation region, and then vary the modal particle size of forsterite grains to create a model set with a wide range of possible cloud optical thicknesses.

To mimic the transformation of a young, cloudy object evolving into an old, cloud-free object, and the L-to-T transition, we linearly combine cloudy ($\mathcal{S}_{\text{cloudy}}$) and cloudfree ($\mathcal{S}_{\text{cloudfree}}$) spectra using the phenomenological prescription:

$$\begin{aligned} \mathcal{W} &= \min\{1, (T_{\text{eff}}/T_0)^p\}, \\ \mathcal{S}_{\text{hybrid}} &= \mathcal{W}\mathcal{S}_{\text{cloudy}} + (1 - \mathcal{W})\mathcal{S}_{\text{cloudfree}}. \end{aligned} \quad (3)$$

Thus, T_0 is the transitional temperature at and below which clouds in the L dwarf atmosphere begin to both disperse and reside below the photosphere, while the power law index p describes the speed of the transition. Effectively, our hybrid models have five parameters: s_u , $s_d = 10$, a_0 , T_0 and p . We are guided by empirical measurements of the color-magnitude diagram to choose $T_0 = 1200$ K and $p = 4$. Although our approach is intrinsically different from f_{sed} parametrization of Saumon & Marley (2008), the resulting cloud structures and temperature profiles are similar across the L-to-T transition.

An evolutionary Henyey code is used to establish the mapping between $\{T_{\text{eff}}, g\}$ and $\{M, t\}$ (mass-age) pairs. With the equation of state (EOS) for hydrogen/helium mixtures of (Saumon, Chabrier, & Van Horn 1995) and specified values of the deuterium and helium fractions, the code solves the equations of stellar structure.

We emphasize that the hydrogen/helium EOS of Saumon, Chabrier, & Van Horn (1995) employs the volume addition law for such mixtures and does not have a rigorous means to incorporate heavy elements in a consistent fashion. Hence, though the core and atmosphere will certainly have the same $[\text{Fe}/\text{H}]$, we do not include heavies in our EOS. Currently, there does not exist a reliable EOS for more complicated mixtures. If the matter were an ideal gas, then one could easily incorporate any range of elemental abundance mixtures by calculating the appropriate mean molecular weight. However, the material in SMOs experiences significant Coulomb interaction effects. Indeed, at the high densities and low entropies encountered in their cores, the Coulomb effects are important. At higher densities, degeneracy effects predominate, and the EOS, depending as it does on the electron fraction per baryon, again simplifies. However, with brown dwarfs we are often in the intermediate regime where Coulomb and degeneracy effects compete, an awkward regime to treat well. At times, theorists have employed altered helium fractions to treat heavies, boosting Y by an ‘‘appropriate’’ amount and then using the H/He EOS with the enhanced Y (Spiegel, Burrows, & Milsom 2011; Guillot et al. 2006). At solar metallicity, $[\text{Fe}/\text{H}] = 0.0142$ and the effect of neglecting heavies in the EOS, while not large, is still interesting. However, the reader should be aware that the results we quote do not automatically incorporate heavies in the core EOS and that the stopgap of using a ‘‘suitably’’ enhanced Y to gauge their effects remains an option. If this be the case, then a $3\times$ solar metallicity would be equivalent to a ~ 0.04 augmentation in Y , comparable to the range of Y we explore in this paper.

The boundary condition between the atmosphere and the convective core is the entropy at the radiative-convective transition layer of the planar atmosphere, which is an output of COOLTLUSTY. By merging the evolutionary and spectral computations in this manner, we ensure that our spectral-evolutionary calculations are self-consistent.

For this investigation, we calculate models from $1 M_J$ to $0.15 M_\odot$ ($\sim 157 M_J$) and focus on three atmospheric metallicities: $[\text{Fe}/\text{H}] = \pm 0.5$ and 0.0 (solar). Hence, our models are 1) clear with the three different metallicities and 2) cloudy hybrid with $[\text{Fe}/\text{H}] = 0.0$ and 0.5 . These five models, along with the heritage model from Burrows et al. (1997), are used to fit the measured radii of the brown dwarfs LHS 6343C, CoRoT-3b, CoRoT-15b, & WASP-30b and the very-low-mass (VLM) stars OGLE-122b and OGLE-123b and to arrive at the various general conclusions.

4. GENERAL THEORETICAL BEHAVIOR

In this section, we discuss the qualitative behavior of both the radius evolution with time and the radius–mass isochrones as a function of the presence or absence of clouds, the atmospheric metallicity, and the helium fraction. The importance of including clouds in evolutionary models was previously emphasized by Saumon & Marley (2008). Figure 1 depicts the temporal evolution of the radii of theoretical brown dwarfs at four different masses (0.055 , 0.060 , 0.065 , and $0.070 M_\odot$, equivalent to ~ 58 , ~ 63 , ~ 68 , and $\sim 73 M_J$) for models with cloudy atmospheres at $[\text{Fe}/\text{H}] = 0.0$ and 0.5 and for cloud-free

atmospheres at $[\text{Fe}/\text{H}] = 0.0$. The cloud model incorporates the cloud prescription described in section 3. Since the physics of cloud particles and structure are not yet understood, this cloud model should be viewed merely as representative of the effects of clouds. However, it is neither extreme in its properties, nor unrealistic, and introduces the extra degree of atmospheric opacity expected of such clouds.

As Fig. 1 indicates, before ~ 1 Gyr brown dwarf radii evolve very quickly, but later their shrinkage moderates significantly. Importantly, however, this figure shows the radius hierarchy that emerges from this study. Models with higher atmospheric opacity, due either to higher metallicity or to the presence of thick clouds, have larger radii at a given mass and age than those with lower opacity. The latter would be associated with lower metallicity and/or the absence of clouds. Importantly, the natural spread in theoretical radii at a given mass and age can be significantly larger than the quoted formal error bars of the measured radii. To demonstrate this, we have superposed onto this figure the data for the three brown dwarfs in the mass range ~ 60 to $\sim 70 M_J$ for which we have useful transit radii and masses (LHS 6343C, WASP-30b, and CoRoT-15b). We caution that the formal error bars in measured radii may be trumped by systematic errors in the observational analysis and that the true error in the data may be larger than published. In turn, there are, no doubt, “errors” in the theoretical models that spring from uncertainties in the gas-phase opacities, uncertainties in the equation of state, elemental abundances patterns for a given metallicity that are different from what is assumed, and the many uncertainties in designing accurate cloud models. Nevertheless, as Fig. 1 demonstrates, for reasonable stellar/(brown dwarf) metallicities expected in the solar neighborhood, the radius spread at a given mass and age can be as large as $\sim 0.2 R_J$. This exceeds any reasonable error stemming from uncertainties in the equation of state alone and serves to emphasize that measurements of brown dwarf radii constrain a collection of effects, importantly including the atmosphere and condensate cloud models. Without an independent measure of the atmospheric metallicity and constraints on the surface clouds, and a good age constraint, a measurement of a brown dwarf radius may be less useful than some might expect for testing the hydrogen/helium equation of state.

One way to understand the effect of enhanced atmospheric opacity on the radius of an SMO is by way of the consequent alteration in atmospheric temperature/pressure profiles (for a given T_{eff} and gravity) with increasing atmospheric metallicity or upon the introduction of clouds. Figure 2 depicts three sets of atmospheric thermal profiles at $T_{\text{eff}} = 1300$ K and five gravities from $\log_{10} g = 3.5$ to $\log_{10} g = 5.5$. The three sets are cloud-free (red), cloudy at solar metallicity (green), and cloudy at $3\times$ solar metallicity (blue). As is clear from the figure, when comparing cloudy with cloud-free models we notice that at a given temperature, the pressure is everywhere lower for the cloudy model. This is also the case when comparing cloudy/solar with the cloudy/ $3\times$ solar models. This indicates that the entropy at depth, the core entropy, is correspondingly higher for the atmospheres with enhanced opacity due either to increased metallicity or the presence of clouds. Since at a given mass

higher entropy translates into larger radii, Fig. 2 neatly demonstrates the opacity/radius connection and our general thesis.

Figure 3 portrays isochrones from 0.5 to 5.0 Gyr in radius–mass space from $1 M_J$ to $120 M_J$ for the “heritage” model published by Burrows et al. (1997). Superposed are the corresponding data for the six objects of this study. There is a slight peak near $\sim 4 M_J$. At larger masses (in the “brown dwarf regime”), radii decrease with increasing mass, monotonically shrinking as they age. Depending upon age, for masses around $\sim 60 M_J$ to $\sim 70 M_J$, the radius then begins to increase with mass. This is a manifestation of the onset of significant thermonuclear burning and the transition to a star. Hence, there is a minimum radius for a given model and age. From 1 Gyr to 5 Gyr that minimum radius ranges from $\sim 1.1 R_J$ to $\sim 0.75 R_J$ for the five-model suite studied in this paper and from $\sim 0.9 R_J$ to $0.77 R_J$ for the Burrows et al. (1997) models. As Fig. 3 shows, OGLE-122b and OGLE-123b are clearly stars, though a comparison with these heritage models requires OGLE-123b to be quite young. However, Pont et al (2005,2006) suggest that the OGLE objects might indeed be younger than 0.5 Gyrs. The quoted age range of LHS 6343 is between one and five billion years (Johnson et al. 2010) and Fig. 3 implies that the Burrows et al. (1997) model set could fit this object. Anderson et al. (2011) suspect that WASP-30b is younger than 1 Gyr, but given the inherent ambiguities in such an estimate Fig. 3 indicates that the Burrows et al. (1997) models might provide an adequate fit. The age of CoRoT-3 is not well constrained and its radius error bars are large, making a comparison between theory and measurement an easy, though rather useless, exercise. However, with a suggested age range of ~ 1.14 – 3.35 Gyr (Bouchy et al. 2011), CoRoT-15b might be the only object among the six we are highlighting in this paper for which a solution using the Burrows et al. (1997) models might be problematic.

Figure 4 compares radius–mass trajectories for cloudy-atmosphere models and clear-atmosphere models at four different ages (0.5, 1.0, 3.0, and 5.0 Gyr). The clear models have atmospheric metallicities ($[\text{Fe}/\text{H}]$) of -0.5 , 0.0 , and $+0.5$, while the cloudy models have atmospheric metallicities of 0.0 and $+0.5$. As Fig. 4 demonstrates, increasing the metallicity increases the radius, with or without clouds. We note that atmospheres without clouds, or a cloud effect, are not expected for metallicities of solar and above. Nevertheless, for clear models at early ages, the spread in radius for brown dwarfs with masses between $\sim 30 M_J$ and $\sim 70 M_J$ and for the metallicity range of this study can be as much as $\sim 0.15 R_J$. For the same clear model set at late ages, that same spread narrows between $\sim 55 M_J$ and $\sim 70 M_J$ to $\sim 0.1 R_J$. For the cloud models, at early ages the radii can range by $\sim 0.15 R_J$ in going from $[\text{Fe}/\text{H}] = 0.0$ to $[\text{Fe}/\text{H}] = 0.5$, but that range tightens at the later ages to $\sim 0.05 R_J$ for the more massive brown dwarfs. However, the spread in radius from clear models at $[\text{Fe}/\text{H}] = -0.5$ to cloudy models at $[\text{Fe}/\text{H}] = 0.5$ can be as large as $\sim 0.25 R_J$ at early ages, and as large as $\sim 0.1 R_J$ at late ages. This implies that each increment in $[\text{Fe}/\text{H}]$ of 0.1 can translate into a radius change of ~ 1 – 2.5 %, depending upon age and mass.

In the stellar realm above $\sim 90 M_J$, atmospheric temperatures are above the condensation temperatures of

iron and refractory silicates. As a consequence, and as we see in Fig. 4, the radii of stars depend only weakly on the presence or absence of clouds. However, their radii are still modest functions of atmospheric metallicity. Increasing the metallicity of a VLM star from 0.0 to 0.5 increases the radius by $\sim 4\%$ and from -0.5 to 0.5 by $\sim 10\%$. The latter percentage is slightly above what is oft-quoted as the discrepancy in radius between measurement and theory in the VLM regime. Though we do not in this investigation discuss models in the $\sim 0.2 M_{\odot}$ to $0.25 M_{\odot}$ band, the implication of the systematic behavior of Fig. 4 in the stellar realm is that opacity due to higher metallicity can naturally account for this apparent radius anomaly in, for instance, the CM Dra (Morales et al. 2009) and KOI-126 (Carter et al. 2011) systems. Neither rotation nor magnetic activity (Chabrier, Gallardo, & Baraffe 2007) need be the only (nor the dominant) explanation. Summarizing, the effect of atmospheric metallicity on the radii of brown dwarfs and VLMs is straightforward and natural, and the magnitude of the potential spread in radii for reasonable ranges in metallicity in the solar neighborhood is comparable to published apparent discrepancies.

Figure 5 recapitulates some of the information on Fig. 4, but highlights the helium fraction dependence of the radius–mass relation and is for only solar atmospheric metallicity. Shown are trajectories for $Y = 0.25$ (blue/aqua) and $Y = 0.28$ (red/magenta), where Y is the helium mass fraction. At zero temperature, the higher the mean molecular weight and the lower the electron-to-baryon ratio (both consequences of higher Y), the smaller the brown dwarf. At later ages and lower masses, Fig. 5 clearly demonstrates this tendency, and this is the widely-expected result. However, for the higher temperatures and entropies which persist for more massive brown dwarfs, the opposite is true – a higher helium fraction leads to a larger radius. The magnitude of the effect is slight, but can amount to as much as $\sim 0.025 R_J$. As Fig. 5 shows, this slight “reversal” continues into the stellar realm. We note that the Burrows et al. (1997) models (also shown on the figure for comparison) were calculated for $Y = 0.25$, but that a value of $Y = 0.28$ is generally preferred (Saumon & Marley 2008).

This slightly counterintuitive result at larger masses is due to the enhanced core hydrogen burning rate for the larger Y , despite the slightly smaller hydrogen fraction. In hydrostatic equilibrium, the fact that at higher mean molecular weight the adiabat is higher results in a higher core temperature for an isentropic core. Hence, larger Y (which translates into a higher mean molecular weight) results in higher central temperatures, which generate higher thermonuclear powers. This also results in higher core entropies for a given convective mass and age, and, hence, larger outer radii. When the nuclear luminosity is very small, the larger Y results in more compact configurations, as is expected from the behavior of the EOS, and smaller outer radii. However, for larger masses, the core temperatures eventually become significant, even if the object is not destined to settle onto the main sequence. The condition for the latter is that the core thermonuclear power equal the atmospheric luminosity – the first mass for which this condition is satisfied defines the main sequence edge. However, even for lower masses, thermonuclear power can retard the decay of the

core entropy, which for a given mass determines the outer radius. That the specific heat decreases with increasing Y is a slightly mitigating effect, but this is trumped by the enhancement in nuclear burning rate. The same phenomenon was identified in Spiegel, Burrows, & Milsom (2011) in the context of deuterium burning.

Figure 6 portrays the ratio of the nuclear luminosity to the surface photon luminosity for representative masses from 0.05 to $0.08 M_{\odot}$ and $Y = \{0.25, 0.28\}$. When this ratio is equal to one we are on the main sequence. As Fig. 6 demonstrates, even for masses near $0.05 M_{\odot}$ and far below the main sequence, core burning is both non-trivial and larger for larger Y . The higher nuclear luminosity for higher Y also helps explain why VLM radii are larger for larger Y (Fig. 5).

We end this section by reiterating that our core EOS does not automatically incorporate the slight effect of metallicity, but that one can approximately account for heavy elements in the EOS by augmenting the helium fraction accordingly. This suggests, given the findings summarized in Fig. 5, that properly including them in the EOS would further (though only slightly) increase the radii of VLMs and of the more massive brown dwarfs younger than ~ 5 Gyrs, emphasizing yet again the potential role of metallicity in influencing SMO radii.

5. MODELS FOR INDIVIDUAL OBJECTS

The six objects (LHS 6343C, WASP-30b, CoRoT-15b, CoRoT-3b, OGLE-TR-122b, and OGLE-TR-123b) that we investigate in this paper have measured transit radii and radial-velocity masses. The errors in the measured radii quoted in the discovery papers are usually purely statistical, yet systematic errors may actually dominate. Therefore, the reader should keep this in mind when we derive approximate physical properties for these objects from a comparison with our theoretical models. There may in fact be more interpretive latitude than we have allowed ourselves. Given this caveat, we now proceed to discuss each individual brown dwarf or VLM.

5.1. LHS 6343C

On Fig. 7, we have plotted four panels in radius–mass space from $40 M_J$ to $80 M_J$, each for a different model set, with and without clouds and for $[\text{Fe}/\text{H}]$ equal to either 0.0 or 0.5. Four isochrones at 0.5, 1.0, 3.0, and 5.0 Gyr are given on each panel. The data from Johnson et al. (2010) for LHS 6343C ($M = 62.9 \pm 2.3 M_J$; $R = 0.833 \pm 0.021 R_J$) are superposed, where the errors are $1-\sigma$. Johnson et al. (2010) suggest an age range from 1 to 5 Gyrs. LHS 6343C is seen to be a small brown dwarf, and, therefore, Fig. 7 suggests that older ages, clearer models, and lower metallicities might be preferred. However, a range of combinations can be shown to fit. For the cloudy model, the older solar-metallicity models may be indicated (bottom right panel). Anderson et al. (2011) suggest a metallicity of 0.28 ± 0.07 , but Johnson et al. (2010) quote 0.04 ± 0.08 . If we were to take the Johnson et al. number and note that low gas-phase metallicity may suggest thinner clouds, we get a consistent set of characteristics in the lower-right-hand panel with an age near 5 Gyrs. Clear models at the higher metallicity fit for an age near $\sim 4\text{--}5$ Gyrs. Clear models at the lower metallicity fit for ages greater than ~ 2 Gyrs (bottom left panel). However, the high-metallicity, cloudy model (top

right panel) does not fit unless the age is greater than ~ 7 Gyrs. Curiously, the Burrows et al. (1997) models (see Fig. 3) fit well for a suggested age of ~ 2 Gyrs.

5.2. WASP-30b

Figure 8 is the same as Fig. 7, but for WASP-30b and with the $[\text{Fe}/\text{H}] = 0.5$ and $[\text{Fe}/\text{H}] = 0.0$ models switched (top \leftrightarrow bottom). Superposed on all panels is the data point for WASP-30b at $60.96 \pm 0.89 M_J$ and $0.89 \pm 0.021 R_J$ (Anderson et al. 2011). The metallicity of WASP-30 is quoted to be $[\text{Fe}/\text{H}] = -0.08 \pm 0.10$, consistent with solar. As Fig. 8 indicates, a variety of models and age–metallicity combinations fit the WASP-30b data. Clear models with $[\text{Fe}/\text{H}] = 0.0$ fit well for ~ 1 – 2 Gyrs. Clear models with $[\text{Fe}/\text{H}] = 0.5$ fit well for ages from ~ 2 to ~ 3 Gyrs. Cloudy models with $[\text{Fe}/\text{H}] = 0.0$ fit well for ages of 3.0 ± 1.0 Gyrs and our cloudy model with $[\text{Fe}/\text{H}] = 0.5$ still fits near ages of ~ 5 Gyrs. Cloudy models with $Y = 0.25$ (not shown) fit at slightly younger ages. As Fig. 3 suggests, the heritage models from Burrows et al. (1997) fit WASP-30b for an age near ~ 1 Gyr. Therefore, as Figs. 8 and 3 together demonstrate, the WASP-30b radius is rather easily fit within its suggested mass, age, and metallicity constraints (soft as they are).

5.3. CoRoT-15b

We superpose the data from Bouchy et al. (2011) for this brown dwarf ($62.9 \pm 2.3 M_J$; $1.12^{+0.30}_{-0.15} R_J$) on Fig. 9, which is in the same format as Fig. 8, but has a slightly different range for the radius and mass axes. CoRoT-15b has the widest error bars for a measured radius among the set of brown dwarfs upon which we focus in this study. Bouchy et al. (2011) estimate a metallicity of 0.1 ± 0.2 (consistent with solar) and an age for its primary in the range ~ 1.14 – 3.35 Gyr. As Fig. 9 suggests, our solar-metallicity models fit in the lower age range to within ~ 1 - σ to ~ 1.5 - σ , with the best fit for the $[\text{Fe}/\text{H}] = 0.0$ cloudy model. However, our $[\text{Fe}/\text{H}] = 0.5$ models fit the suggested age range better, with the clear $[\text{Fe}/\text{H}] = 0.5$ models fitting an age of ~ 1 Gyr to within ~ 1 - σ and the cloudy $[\text{Fe}/\text{H}] = 0.5$ models fitting anywhere in the suggested age range. Cloudy models with $[\text{Fe}/\text{H}] = 0.0$ and clear models with $[\text{Fe}/\text{H}] = 0.5$ fit CoRoT-15b almost equally well. Figure 3 indicates that the Burrows et al. (1997) solar-metallicity models would fit only for very young ages less than ~ 0.5 Gyrs. If the “highish” value of the radius survives, a high-opacity atmosphere model, either due to high metallicity or thick clouds or both, may be indicated for CoRoT-15b. However, the range of possible models available to fit this object remains comfortably broad, particularly for ages younger than ~ 2 Gyrs.

5.4. CoRoT-3b

Figure 10 is similar to Figs. 7, 8, and 9, but is constructed for CoRoT-3b and has a lower mass range between 5 and 40 M_J . Deleuil et al. (2008) measure the mass of CoRoT-3b to be $21.66 \pm 1.0 M_J$ and its radius to be $1.01 \pm 0.07 R_J$. CoRoT-3 has an estimated metallicity of -0.02 ± 0.06 and, hence, the models with solar metallicity may best describe the data. Note that due to the large uncertainty in its radius, many models, both clear and cloudy with a variety of age–metallicity pairs, can fit

CoRoT-3b comfortably. Deleuil et al. (2008) quote an age near ~ 2 Gyr. Fortunately or unfortunately, due to the large radius error bars, all the model sets plotted (cloudy and clear, $[\text{Fe}/\text{H}] = 0.0$ and 0.5) fit the CoRoT-3b data reasonably well. Higher metallicity/cloudy models favor older ages and low metallicity/clear models favor younger ages, but ages between 1 and 5 Gyr are consistent with the quoted mass/radius data for the putative estimated age and metallicity. In addition, as Fig. 3 demonstrates, the Burrows et al. (1997) models fit for any age younger than ~ 6 Gyrs.

5.5. OGLE-TR-122b and OGLE-TR-123b

Figure 11 compares the measured radius–mass points for the VLM stars OGLE-TR-122b and OGLE-TR-123b with cloudy and clear models at ages of from 0.5 to 5.0 Gyrs and for the $[\text{Fe}/\text{H}] = 0.0$ and 0.5 . Pont et al. (2005,2006) suggest that the ages of these VLMs are probably less than 0.5 Gyrs. If this is the case, as Fig. 11 suggests, most of our models provide acceptable fits, with the best fits for OGLE-TR-123b given by either the cloudy or the clear models with $[\text{Fe}/\text{H}] = 0.5$.³ Higher metallicities would fit OGLE-TR-123b even better, but all models fit OGLE-TR-122b. The large radius error bars, as well as the ambiguity in the age of the systems, limit the strength of any general conclusions. Moreover, given the difficulty of these measurements, one should not discount the possibility that these radii might be revised in the future. Not shown on Fig. 11 are models for $[\text{Fe}/\text{H}] = -0.5$ (see Fig. 4), which predict slightly smaller radii at a given mass and age. Nevertheless, whatever the age of these OGLE stars, and in this stellar mass realm, the set of different models (all reasonable in their character and inputs) we have calculated allow a spread in expected radii of $\sim 10\%$.

6. DISCUSSION AND CONCLUSIONS

In this paper, we have generated a collection of evolutionary models for brown dwarfs and very-low-mass stars for different atmospheric metallicities, with and without clouds. These models employ realistic atmosphere boundary conditions that allow us to consistently predict, given a detailed opacity model, the evolution of the object’s radius. We have sought to demonstrate that with transit or eclipse radius measurements one is testing a multi-parameter theory, and not a universal radius–mass relation. The spread in radius at a given mass can be as large as $\sim 0.1 R_J$ to $\sim 0.25 R_J$ (or $\sim 10\%$ to $\sim 25\%$), with higher-metallicity, higher-cloud-thickness atmospheres resulting quite naturally in larger radii, all else being equal. For each 0.1 dex increase in atmospheric $[\text{Fe}/\text{H}]$, the radius is expected to increase by $\sim 1\%$ to $\sim 2.5\%$, depending upon age and mass. Therefore, in order to constrain the hydrogen-helium equation of state one must control for the metallicity and cloud model. If the goal is to test structural theory and the viability of a suite of theoretical models, absent measurements of, for example, the metallicity, and a good constraint on the age, any radius measurement is of cor-

³ Recall that in the putative mass regime of these stars, the atmospheric temperatures are near or above the silicate and iron condensation temperatures. As a result, the differences between cloudy and clear models are minimal.

respondingly limited utility. Conversely, one should expect a range of radii for the natural range of metallicities and possible cloud properties expected for substellar objects and VLM stars in the solar neighborhood.

In addition, we have calculated the effect of helium fraction on brown dwarf and VLM radii and find that, while for smaller masses and older ages radius decreases with increasing helium fraction (as expected), for more massive brown dwarfs and a wide range of ages it increases with helium fraction. This runs counter to common lore, which expects that higher mean molecular weights universally result in smaller radii. We find that the increase in radius in going from $Y = 0.25$ to $Y = 0.28$ can be as large as $\sim 0.025 R_J$ ($\sim 2.5\%$). Furthermore, we suggest that properly including the trace of heavy elements in the core EOS should further augment this effect.

We do not suggest that the cloud model we constructed for this investigation is definitive, nor uniquely applicable. Rather, we engineered a cloud model, and its corresponding opacities and optical depths, to be representative of the generic effect of the clouds we know reside in brown dwarf atmospheres. We have sought merely to demonstrate that the presence or absence of clouds has an important effect on the radius of a brown dwarf. We note that many other cloud models can be constructed which may prove in the long run to be more viable. Nevertheless, the qualitative effect of clouds that we have highlighted is robust. Similarly, and more straightforwardly, atmospheric metallicity has a direct and clear effect on brown dwarf radii that needs to be accounted for in any interpretation of radius measurements.

Ten to twenty-five percent variations in radius exceed any reasonable error stemming from uncertainties in the

equation of state alone and serve to emphasize that measurements of brown dwarf radii constrain a collection of effects, importantly including the atmosphere and condensate cloud models. Without an independent measure of the atmospheric metallicity, constraints on the surface clouds, and a good age estimate, a measurement of a brown dwarf radius may be more difficult to interpret than previously thought.

Increasing the atmospheric metallicity of the VLM stars we studied in this paper from 0.0 to 0.5 increases their radii by $\sim 4\%$. If we increase their atmospheric metallicity from -0.5 to 0.5, their radii increase by $\sim 10\%$. The latter percentage is slightly above what is often quoted as the discrepancy in radius between measurement and theory in the VLM regime (Morales et al. 2009; Carter et al. 2011). Though we do not in this paper discuss models in the $\sim 0.2 M_\odot$ to $0.25 M_\odot$ band, the clear implication of the systematic behavior we have derived in the stellar realm is that opacity due to higher metallicity might naturally account for the apparent radius anomalies in some eclipsing VLM systems.

Be that as it may, the effect of metallicity and clouds on the radii of brown dwarfs and VLMS is straightforward and natural. Therefore, we suggest it is necessary to incorporate these extra degrees of freedom into any interpretation of brown dwarf and VLM radius measurements and into any attempts usefully to constrain their equation of state.

We acknowledge useful conversations with Dave Spiegel and Nikku Madhudsudhan, and Ivan Hubeny for his general support of the COOLTLUSTY code. We also acknowledge support in part under NASA ATP grant NNX07AG80G, HST grants HST-GO-12181.04-A and HST-GO-12314.03-A, and JPL/Spitzer Agreements 1417122, 1348668, 1371432, and 1377197.

REFERENCES

- Allende-Prieto, C., Lambert, D.L., & Asplund, M. 2001, *ApJ*, 556, L63
- Allende-Prieto, C. & Lambert, D.L. 2005, Workshop on Oxygen in the Earliest Solar System, LPI Contribution No. 1278, 9.
- Anders, E. & Grevesse, N. 1989, *Geochim. Cosmochim. Acta*, 53, 197
- Anderson, D.R. et al. 2011, *ApJ*, 726, L19 (arXiv:1010:3006)
- Asplund, M., Grevesse, N., Sauval, A.J., Allende-Prieto, C., & Blomme, R. 2005, *A&A*, 431, 693
- Baglin, A., Auvergne, M., Boissard, L., Lam-Trong, T., Barge, P., Catala, C., Deleuil, M., Michel, E., & Weiss, W. 2006, 36th COSPAR Scientific Assembly, 36, 3749.
- Bakos, G.A., Lázár, J., Papp, I., Sári, P., & Green, E.M. 2002, *PASP*, 114, 974
- Baraffe, I., Chabrier, G., Allard, F., & Hauschildt, P.H. 1998, *A&A*, 337, 403
- Baraffe, I., Chabrier, G., Barman, T., Allard, F., & Hauschildt, P.H. 2003, *A&A*, 402, 701
- Borucki, W. et al. 2010, *Science*, 327, 977
- Bouchy, F. et al. 2011, *A&A*, 525, 68 (arXiv:1010.0179)
- Burgasser, A.J., Burrows, A., & Kirkpatrick, J.D. 2006, *ApJ*, 639, 1095
- Burrows, A., Hubbard, W.B., Saumon, D., & Lunine, J.I. 1993, *ApJ*, 406, 158
- Burrows, A., Marley, M., Hubbard, W. B., Lunine, J.I., Guillot, T., Saumon, D., Freedman, R., Sudarsky, D., & Sharp, C. 1997, *ApJ*, 491, 856
- Burrows, A. & Sharp, C.M. 1999, *ApJ*, 512, 843
- Burrows, A., Hubbard, W.B., Lunine, J.I., & Liebert, J. 2001, *Rev. Mod. Phys.*, 73, 719
- Burrows, A., Sudarsky, D., & Hubeny, I. 2006, *ApJ*, 640, 1063
- Burrows, A., Hubeny, I., Budaj, J., & Hubbard, W.B. 2007, *ApJ*, 661, 502
- Carter, J.A. et al. 2011, *Nature*, in press (arXiv:1102.0562)
- Chabrier, G. & Baraffe, I. 1997, *A&A*, 327, 1039
- Chabrier, G., Gallardo, J., & Baraffe, I. 2007, *A&A*, 472, L17
- Deleuil, M. et al. 2008, *A&A*, 491, 889
- Guillot, T., Santos, N.C., Pont, F., Iro, N., Melo, C., & Ribas, I. A & A, 453, L21, 2006
- Hubeny, I. 1988, *Comput. Phys. Commun.*, 52, 103
- Hubeny, I. & Lanz, T. 1995, *ApJ*, 439, 875
- Johnson, J.A., Apps, K., Gazak, J.Z., Crepp, J., Crossfield, I.J., Howard, A.W., Marcy, G.W., Morton, T.D., Chubak, C., and Isaacson, H. 2010, submitted to *ApJ*(arXiv:1008.4141)
- Koch, D.G. et al. 2010, *ApJ*, 713, L79
- Konacki, M., Torres, G., Jha, S., & Sasselov, D. 2003, *Nature*, 421, 507
- Konopacky, Q.M., Ghez, A.M., Barman, T.S., Rice, E.L., Bailey, J.I., White, R.J., McLean, I.S., & Duchêne, G. 2010, *ApJ*, 711, 1087
- Liu, M.C., Dupuy, T.J., & Leggett, S.K. 2010, *ApJ*, 722, 311
- Morales, J.C. et al. 2009, *ApJ*, 691, 1400
- Pollacco, D. et al. 2004, *MNRAS*, 355, 1576
- Pont, F., Melo, C.H.F., Bouchy, F., Udry, S., Queloz, D., Mayor, M., & Santos, N.C. 2005, *A&A*, 433, L21
- Pont, F., Moutou, C., Bouchy, F., Behrend, R., Mayor, M., Udry, S., Queloz, D., Santos, N., & Melo, C. 2006, *A&A*, 447, 1035
- Saumon, D., Chabrier, G., & Van Horn, H. 1995, *ApJS*, 99, 713
- Saumon, D. & Marley, M.S. 2008, *ApJ*, 689, 1327
- Sharp, C.M. & Burrows, A. 2007, *ApJS*, 168, 140
- Spiegel, D., Burrows, A., & Milsom, J.A.. 2011, *ApJ*, 727, 57
- Stassun, K.G., Mathieu, R.D., & Valenti, J.A., 2006, *Nature*, 440, 311

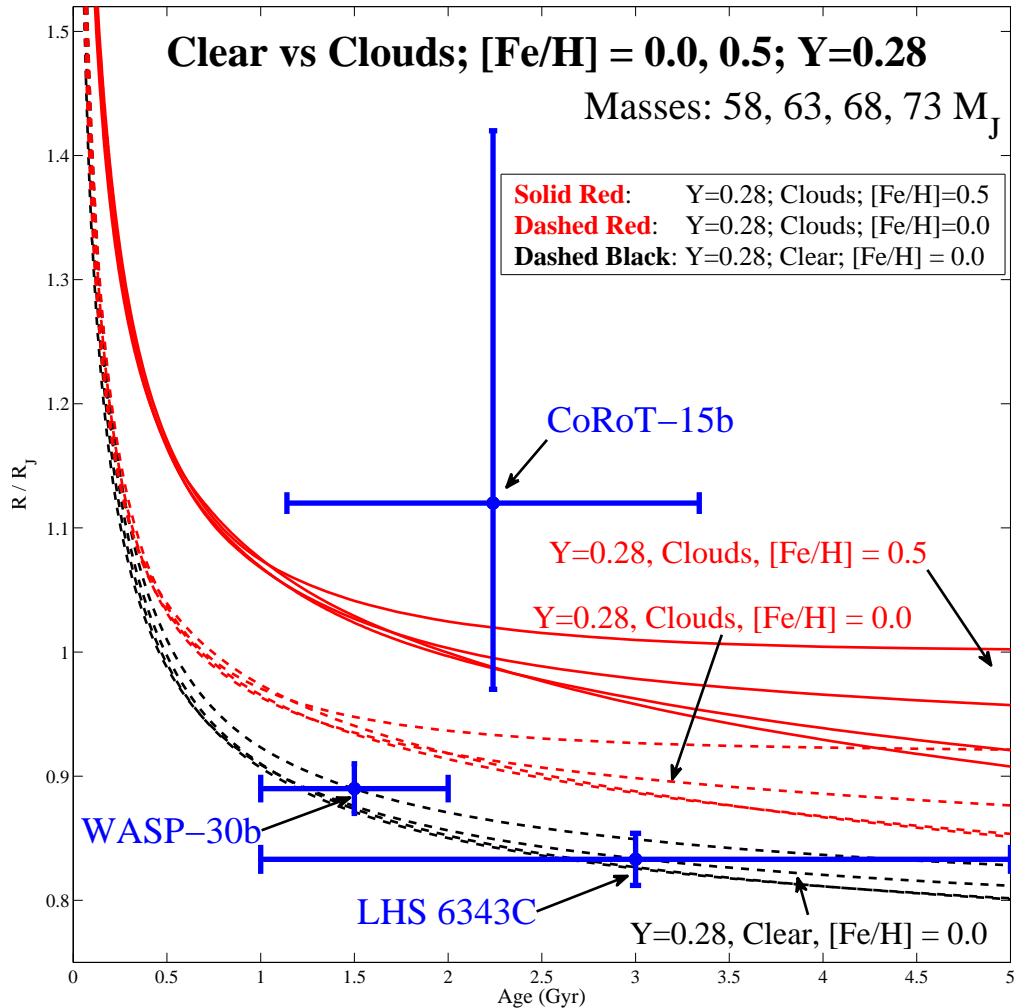


FIG. 1.— The evolution with age (in Gyrs) of the radii (in units of Jupiter’s radius) of brown dwarfs for representative models with 1) cloudy atmospheres (at $[\text{Fe}/\text{H}] = 0.0$ [dashed] and 0.5 [solid], shown in red) and 2) clear atmospheres (at $[\text{Fe}/\text{H}] = 0.0$ [dashed], shown in black). (See section 3 for a discussion of the cloud prescription.) The four masses shown are 0.055 , 0.060 , 0.065 , and 0.070 solar mass (or approximately 58 , 63 , 68 , and 73 Jupiter masses). The helium mass fraction (Y) for each model is here set to 0.28 , i.e., roughly the solar value. This figure shows that the radius of a brown dwarf is an increasing function of metallicity and is larger for models with clouds, all else being equal. Three of the brown dwarfs which we highlight in this paper (LHS 6343C, WASP-30b, and CoRoT-15b) have masses within this range and are included (in blue) on the figure, with putative observational error bars. The formal errors in the age are the most uncertain. As this figure indicates, before ~ 1 Gyr, the radius evolves quickly, but afterwards significantly decelerates its shrinkage.

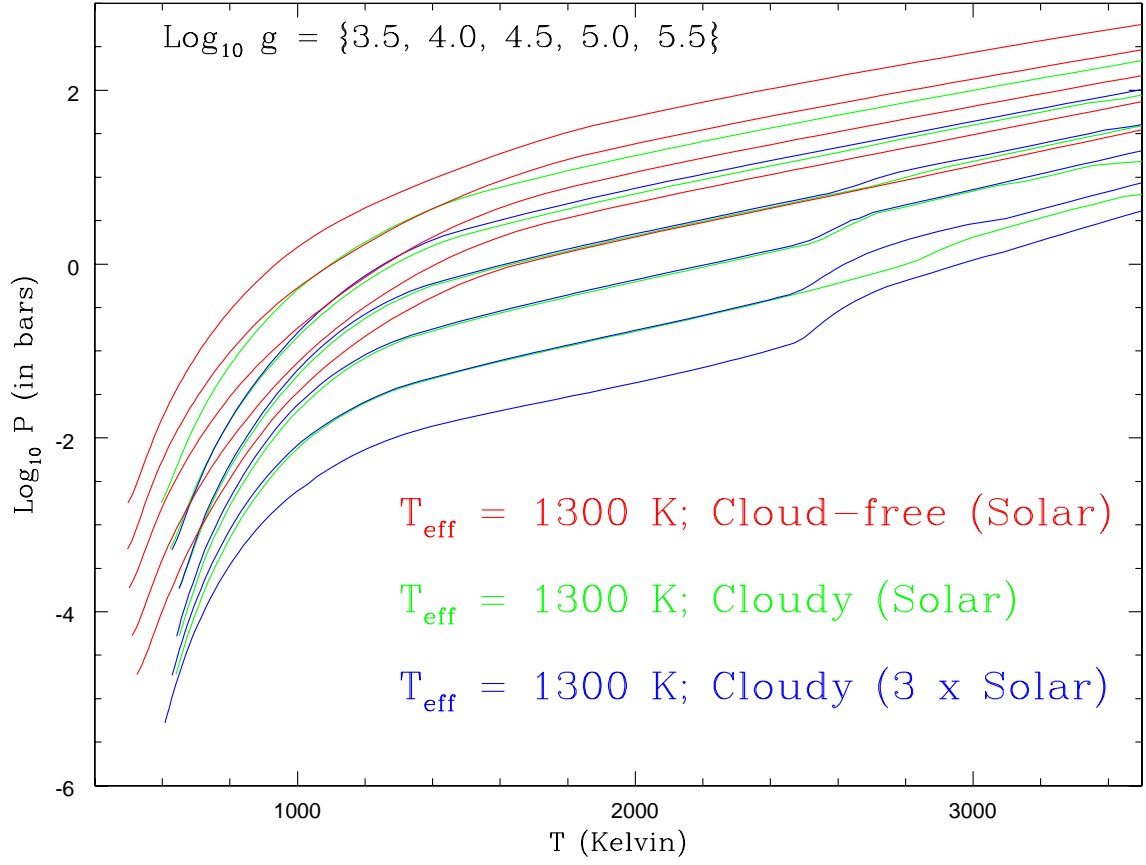


FIG. 2.— This figure depicts three sets of atmospheric thermal profiles for $T_{\text{eff}} = 1300 \text{ K}$ and five gravities from $\log_{10} g = 3.5$ to $\log_{10} g = 5.5$. The three sets are cloud-free (red), cloudy at solar metallicity (green), and cloudy at $3\times$ solar metallicity (blue). The pressure is in bars and is logarithmically displayed and the temperature is in Kelvin. At given T_{eff} and for a given model set, the higher gravity profiles are those with higher pressures. See text in section 4 for a discussion of the import and meaning of this figure.

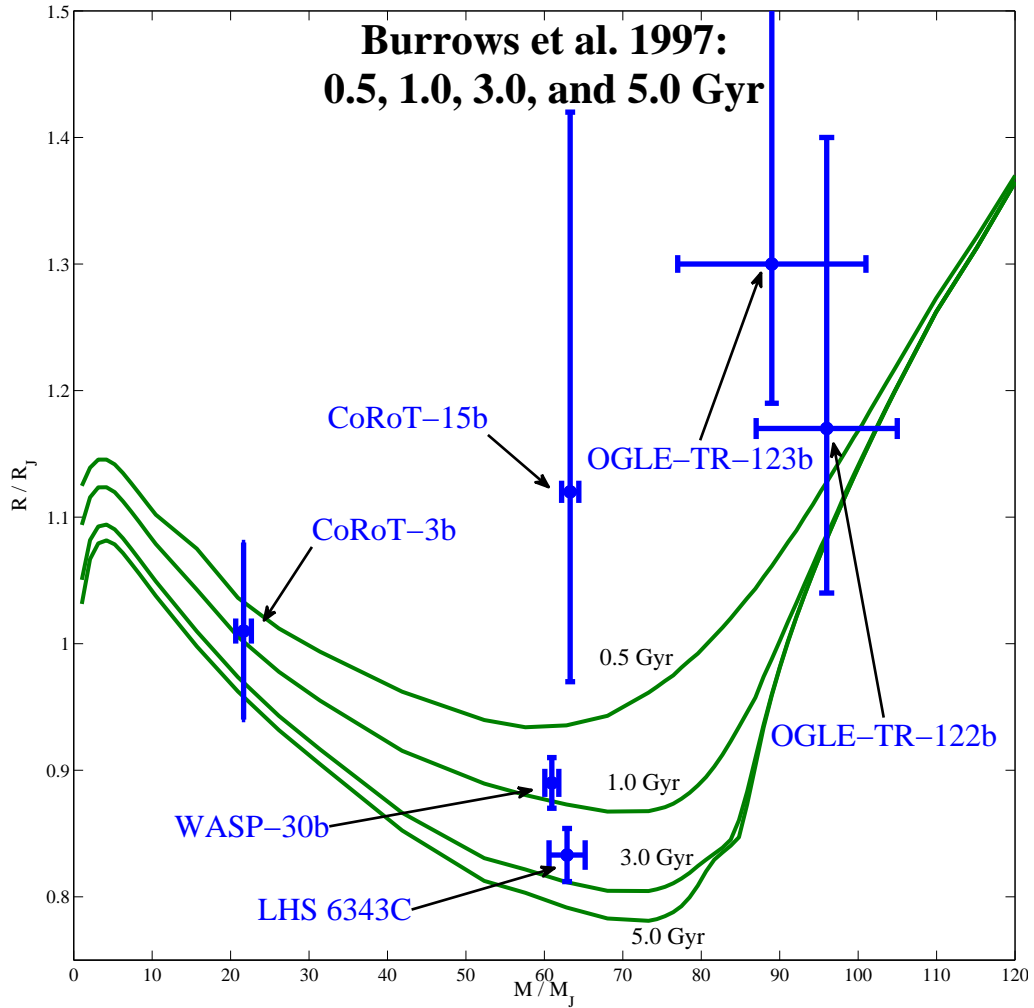


FIG. 3.— Radius (in units of Jupiter’s radius) versus Mass (in Jupiter masses) using the Burrows et al. (1997) “heritage models” at ages 0.5, 1.0, 3.0, and 5.0 Gyr. Notice the slight peak near $\sim 4 M_J$, the decrease in radius with increasing mass in the “brown dwarf regime” at greater masses, and the monotonic radius shrinkage with increasing age. The curves start to rise near the main-sequence edge (near $\sim 75 M_J$) and OGLE-122b and OGLE-123b are clearly stars. Six objects (four brown dwarfs, two VLMs) are shown in blue (with putative mass and age error bars): LHS 6343C (Johnson et al. 2010), WASP-30b (Anderson et al. 2011), CoRoT-3b (Deleuil et al. 2008), CoRoT-15b (Bouchy et al. 2011), OGLE-TR-122b (Pont et al. 2005), and OGLE-TR-123b (Pont et al. 2006). The quoted age of LHS 6343 is between one and five billion years. WASP-30b is suspected to be younger (see Fig.1). Pont et al (2005,2006) suggest that the OGLE objects might be younger than 0.5 Gyrs, and, hence, their measured radii might be consistent with these models. The age of CoRoT-3 is not well constrained. Therefore, with the suggested age range of $\sim 1.14\text{--}3.35$ Gyr for the star CoRoT-15 (Bouchy et al. 2011), CoRoT-15b is the only object in this set for which a solution using these heritage models may be problematic. See the text for a discussion.

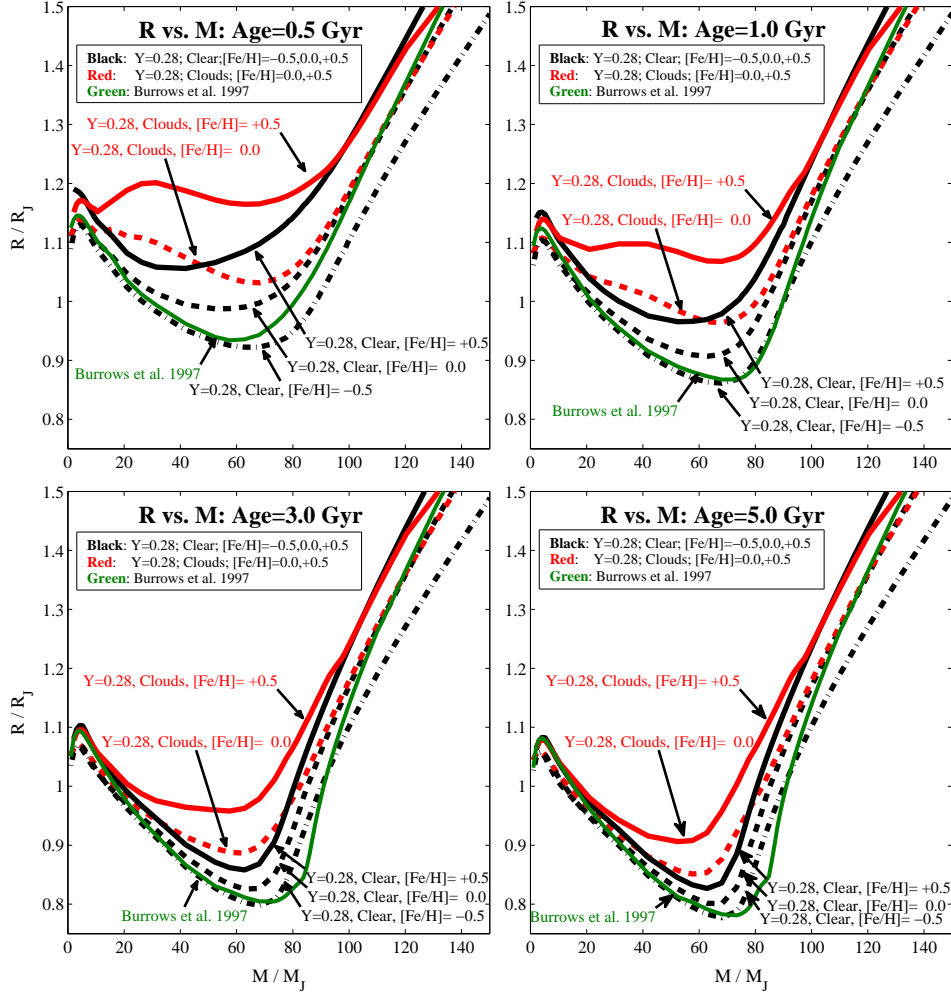


FIG. 4.— Plots of radius (in Jupiter radii) versus mass (in Jupiter masses) at ages of 0.5 (top left), 1.0 (top right), 3.0 (bottom left), and 5.0 (bottom right) Gyr for several new models, all with $Y = 0.28$. The heritage models from Burrows et al. (1997) (in green) are included for comparison. Cloudy-atmosphere models are shown in red and clear-atmosphere models are shown in black. The clear-atmosphere models have metallicities ($[\text{Fe}/\text{H}]$) of -0.5 , 0.0 , and $+0.5$, while the cloudy-atmosphere models have metallicities of 0.0 and $+0.5$. A general trend is that the presence of clouds retards shrinkage, as does higher metallicity. The model with $[\text{Fe}/\text{H}] = 0.5$ and a cloudy atmosphere generally has the largest radii and the variation in radii among the models shown can be $0.1\text{--}0.25 R_J$ at a given mass and age.

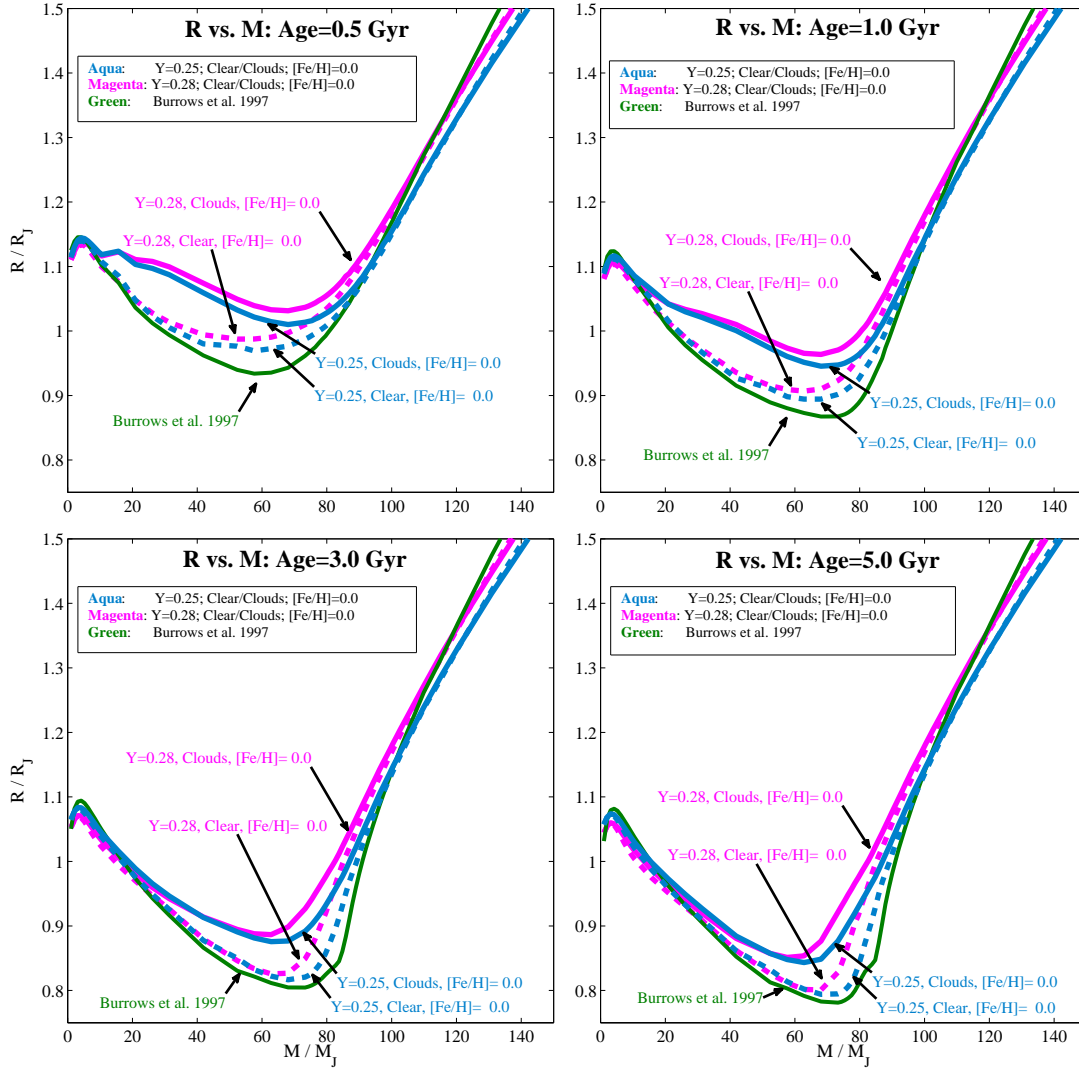


FIG. 5.— Similar to Fig. 4, but highlighting the differences between models with two different helium fractions, $Y = 0.25$ (blue/aqua) and $Y = 0.28$ (magenta). The gas-phase metallicity is solar for all models shown. As a reference, the model from Burrows et al. (1997) is also plotted (in green). The solid lines represent models with clouds, while the dashed lines are those with clear atmospheres. The solid (cloudy) models are generally larger than the corresponding dashed (clear) models. Interestingly, the magenta ($Y = 0.28$) models are larger than the blue/aqua ($Y = 0.25$) models in the mass range above $\sim 55-60 M_J$ at later ages (3.0 and 5.0 Gyr) and above $\sim 35-40 M_J$ at earlier ages (0.5 and 1.0 Gyr). This is counter to common lore, which suggests that planets with a higher molecular weight and lower electron fraction should be smaller. This is true only for cold planets. Note that the Burrows et al. (1997) models were calculated for $Y = 0.25$ (Saumon & Marley 2008). See text for a discussion.

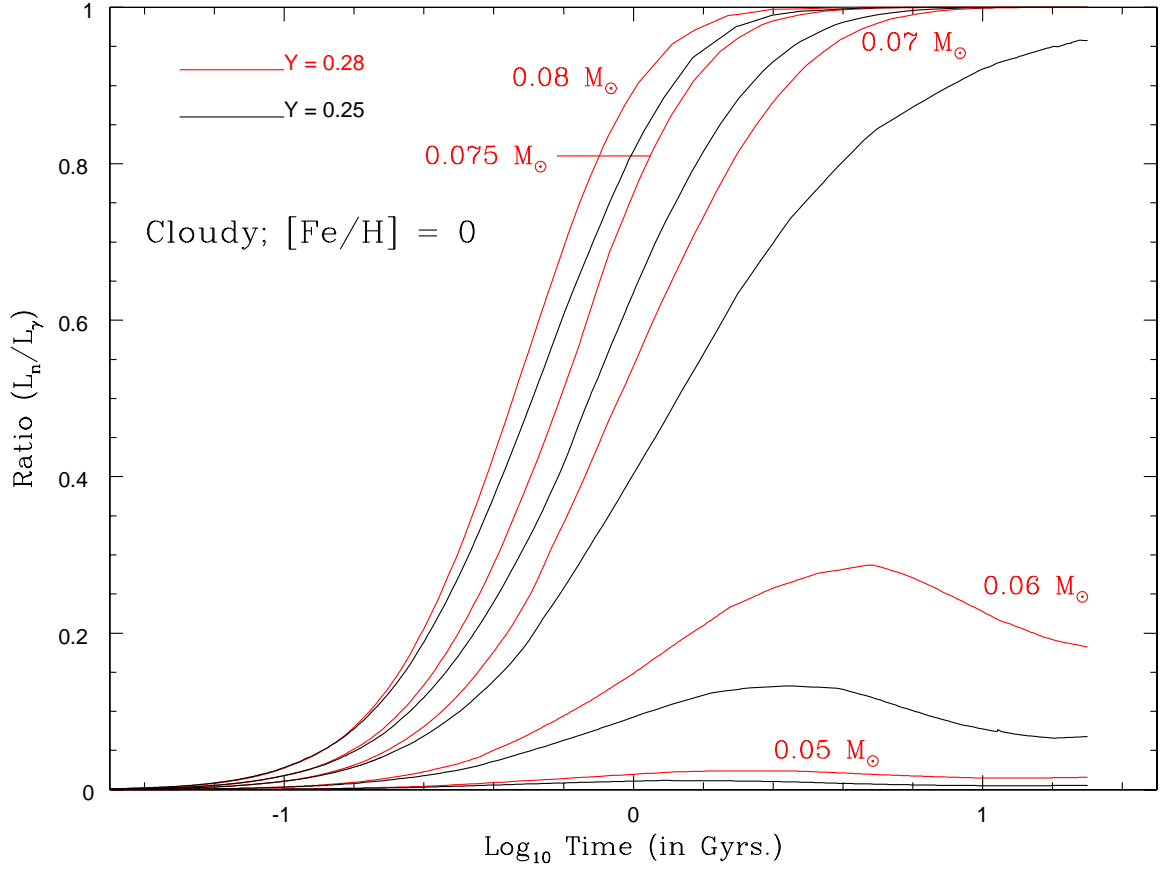


FIG. 6.— The ratio of the core nuclear power to the surface photon luminosity versus age/time (in Gyrs.) for masses of 0.05, 0.06, 0.07, 0.075, and 0.08 M_\odot . The main sequence obtains when this ratio is one. The red lines are for $Y = 0.28$ and the black lines are for $Y = 0.25$. The mass of a given model is printed nearest the relevant $Y = 0.28$ (red) line. The corresponding $Y = 0.25$ (black) line is always below the $Y = 0.28$ line. The solar-metallicity cloudy atmosphere model was used. As this figure demonstrates, even for masses near 0.05 M_\odot and far below the main sequence edge, core burning is both non-trivial and larger for larger Y . The fact that the nuclear power is higher for higher Y also helps explain why VLM radii are larger for larger Y (refer to Fig. 5). See text for a discussion.

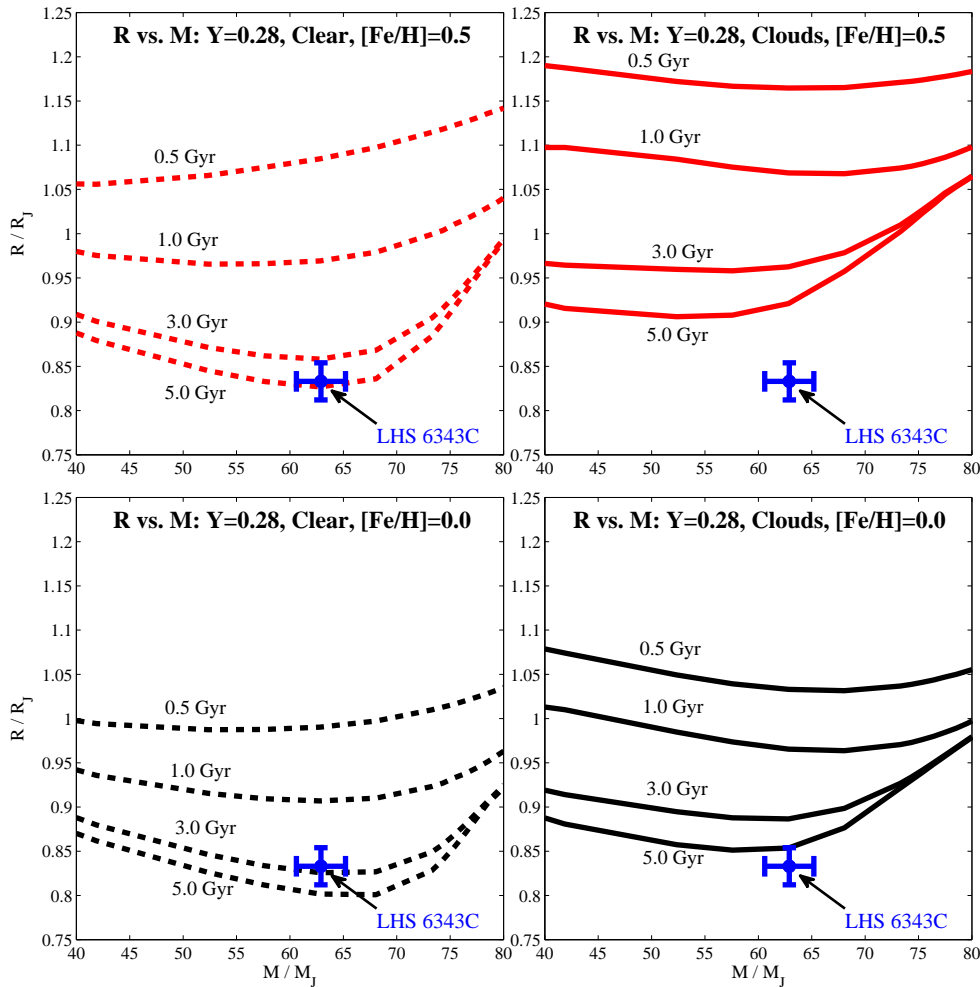


FIG. 7.— LHS 6343C Study: Radius (in units of Jupiter’s radius) versus mass (in units of Jupiter’s mass) for clear models (left panels) and cloudy models (right panels) for $[Fe/H] = 0.5$ (top two panels) and $[Fe/H] = 0.0$ (bottom two panels). All the models shown are for a helium fraction, Y , of 0.28. On each panel are shown isochrones at 0.5, 1.0, 3.0, and 5.0 Gyrs. Superposed on all panels is the data point for LHS 6343C at $62.9 \pm 2.3 M_J$ and $0.833 \pm 0.021 R_J$ (Johnson et al. 2010). The metallicity of LHS 6343C’s primary, LHS 6343A, is suggested by Anderson et al. (2011) to be $[Fe/H] = 0.28 \pm 0.07$, i.e. super-solar, but Johnson et al. (2010) quote a value of 0.04 ± 0.08 . Clear models for $[Fe/H] = 0.0$ (solar) and $[Fe/H] = 0.5$ metallicities fit for ages greater than ~ 2 Gyrs, but the cloudy model with $Y = 0.28$ and $[Fe/H] = 0.0$ also fits for late ages. Models with $Y = 0.25$ fit slightly better, but given the systematic observational uncertainties, nothing substantive can be said about Y for LHS 6343C. The new model with clouds and super-solar metallicity does not fit for ages less than ~ 7 Gyr. As Fig.3 demonstrates, the Burrows et al. (1997) models fit well for the suggested age of ~ 2 Gyrs. See the text for a discussion of the implications of all these model comparisons.

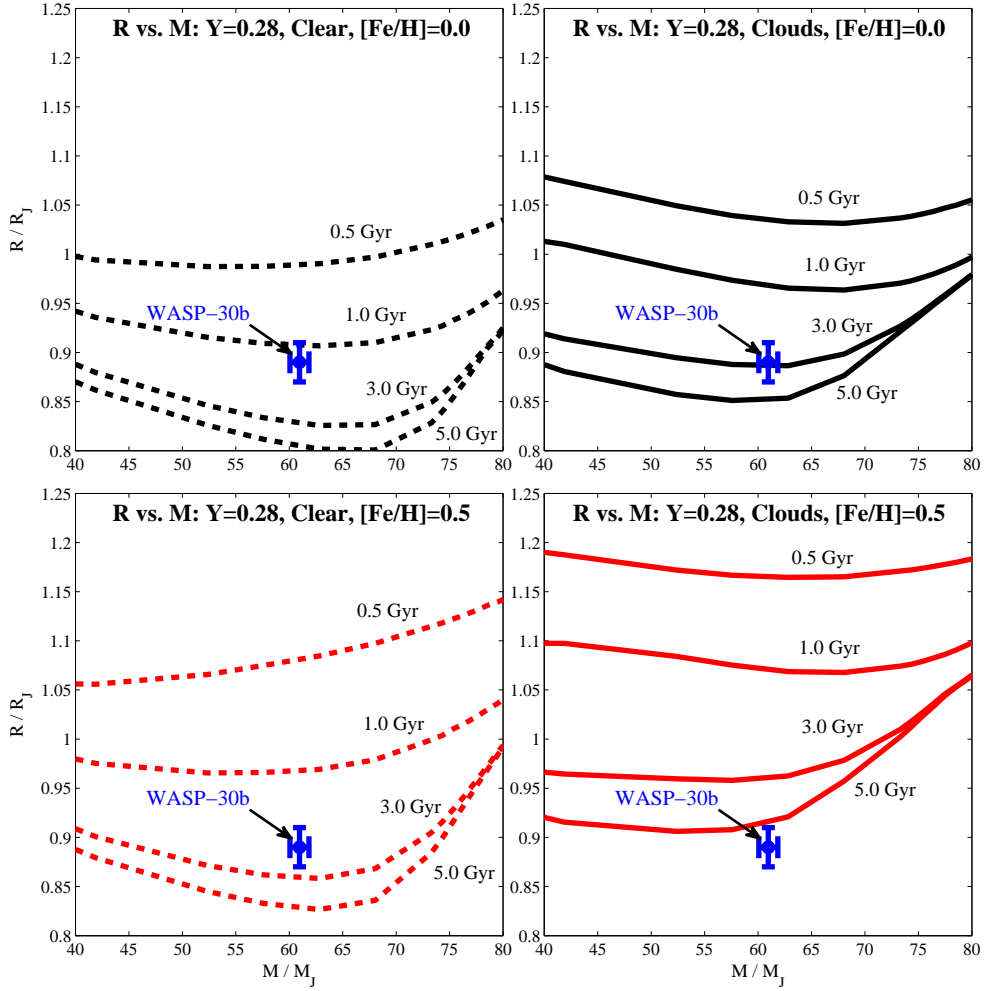


FIG. 8.— Similar to Fig. 7, but for WASP-30b and with the $[\text{Fe}/\text{H}] = 0.5$ models at the bottom and the $[\text{Fe}/\text{H}] = 0.0$ models at the top. (Note that a slightly different range of radii on the ordinate is used.) As in Fig. 7, all the models shown are for a helium fraction of 0.28 and isochrones at 0.5, 1.0, 3.0, and 5.0 Gyrs are plotted. Superposed on all panels is the data point for WASP-30b at $60.96 \pm 0.89 M_J$ and $0.89 \pm 0.021 R_J$ (Anderson et al. 2011). The metallicity of WASP-30 is quoted to be $[\text{Fe}/\text{H}] = -0.08 \pm 0.10$, basically solar. A variety of models and age-metallicity combinations fit the WASP-30b data. Clear models with $[\text{Fe}/\text{H}] = 0.0$ fit well for ~ 1 – 2 Gyrs. Clear models with $[\text{Fe}/\text{H}] = 0.5$ fit well for ages from ~ 2 to ~ 3 Gyrs. Cloudy models with $[\text{Fe}/\text{H}] = 0.0$ fit well for ages of 3.0 ± 1.0 Gyrs and our cloudy model with $[\text{Fe}/\text{H}] = 0.5$ still fits near ages of ~ 5 Gyrs. Cloudy models with $Y = 0.25$ fit at slightly younger ages. As Fig. 3 suggests, the heritage models from Burrows et al. (1997) fit WASP-30b for an age near ~ 1 Gyr. See the text for a discussion of these fits and conclusions concerning WASP-30b.

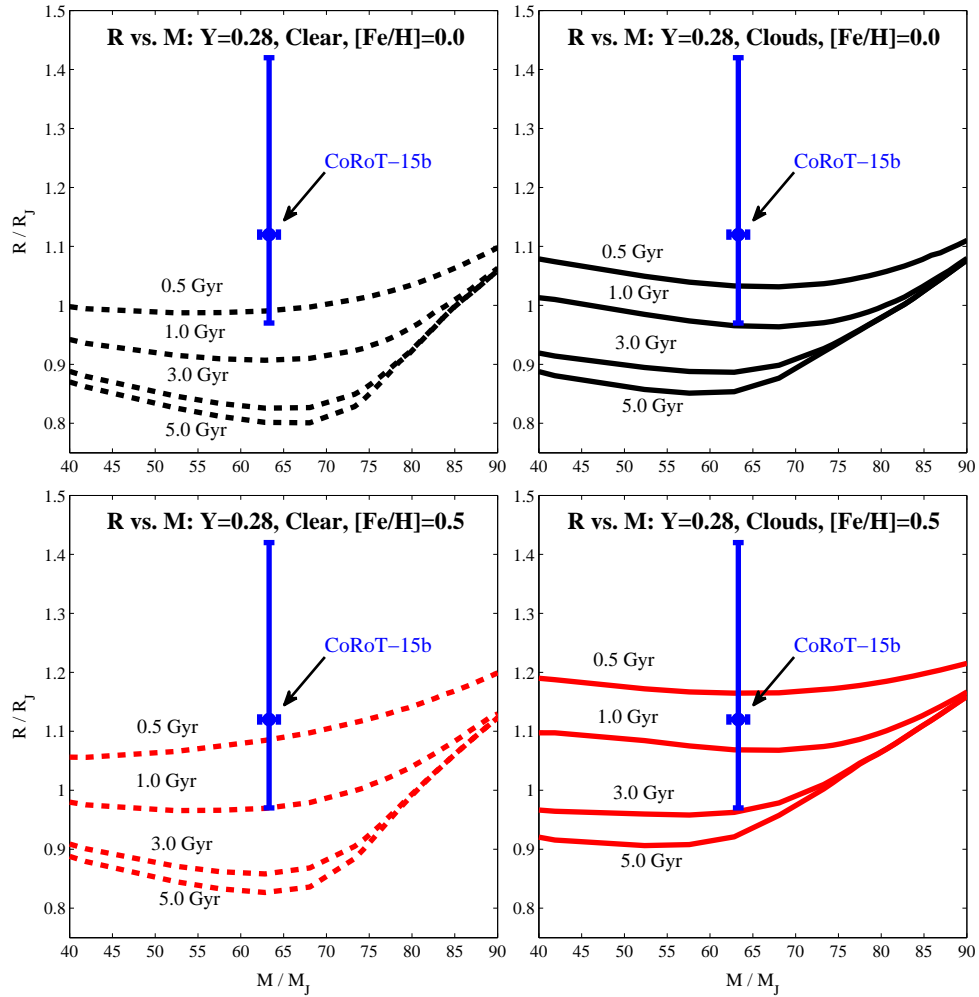


FIG. 9.— Same as Fig. 8, but for CoRoT-15b and with slightly different ranges for the radius and mass axes. The mass of CoRoT-15b is measured to be $62.9 \pm 2.3 M_J$ and its radius is measured to be $1.12^{+0.30}_{-0.15} R_J$ (Bouchy et al. 2011). CoRoT-15 has an estimated metallicity of 0.1 ± 0.2 , again basically solar. Bouchy et al. (2011) suggest that its parent star has an age in the range ~ 1.14 – 3.35 Gyr. Our solar-metallicity ($[Fe/H] = 0.0$) models can fit the lower age range to ~ 1 - σ to ~ 1.5 - σ , with the best fit for the $[Fe/H] = 0.0$ cloudy model. However, our $[Fe/H] = 0.5$ models fit the suggested age range better, with the clear $[Fe/H] = 0.5$ models fitting an age of ~ 1 Gyr within ~ 1 - σ and the cloudy $[Fe/H] = 0.5$ models fitting anywhere in the suggested age range. Cloudy models with $[Fe/H] = 0.0$ and clear models with $[Fe/H] = 0.5$ fit CoRoT-15b almost equally well. Figure 3 suggests that the Burrows et al. (1997) solar-metallicity models would fit only for very young ages less than ~ 0.5 Gyrs. See the text for details.

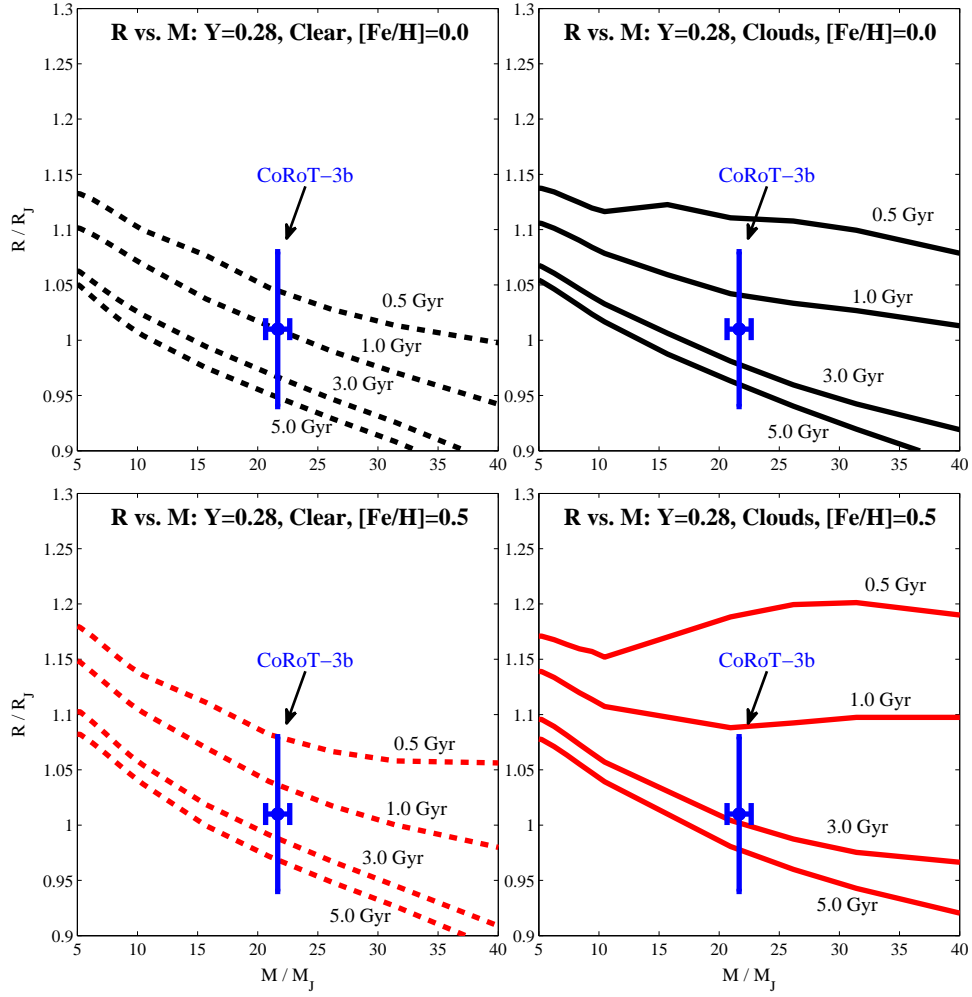


FIG. 10.— Similar to Figs. 7, 8, and 9, but for CoRoT-3b and for a lower brown-dwarf mass range between 5 and 40 M_J . The clear models are on the left panels and the cloudy models are on the right panels. The top models are for $[\text{Fe}/\text{H}] = 0.0$ and the bottom models are for $[\text{Fe}/\text{H}] = 0.5$. The measured mass of CoRoT-3b is $21.66 \pm 1.0 M_J$ and its measured radius is $1.01 \pm 0.07 R_J$ (Deleuil et al. 2008). See text for a discussion.

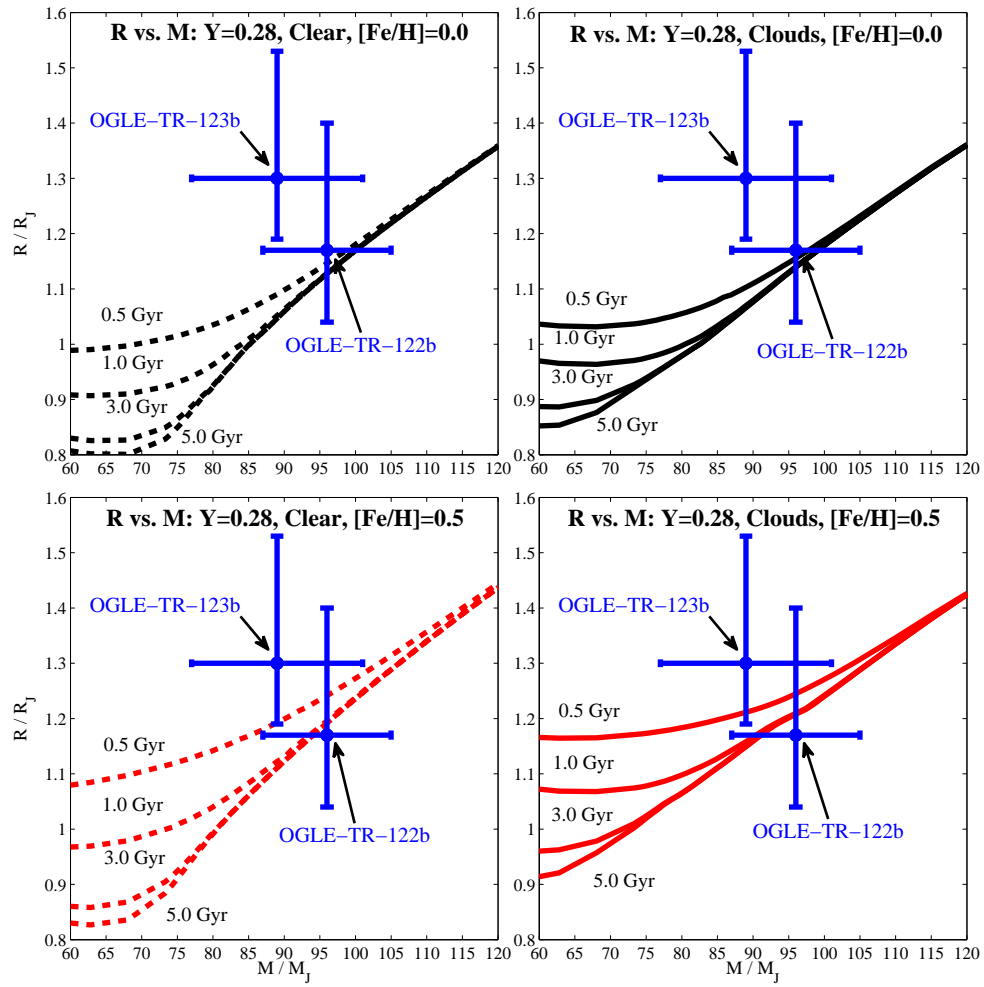


FIG. 11.— Similar to the four previous four-panel figures, the corresponding theoretical radius (in R_J) versus mass (in M_J) model set for OGLE-TR-122b and OGLE-TR-123b. Four isochrones at 0.5, 1.0, 3.0, and 5.0 Gyrs are provided for the $[\text{Fe}/\text{H}] = 0.0$ (top panels) and 0.5 (bottom panels) and for clear (left panels) and cloudy (right panels) models. The data for OGLE-TR-122b and OGLE-TR-123b are taken from Pont et al. (2005) and Pont et al. (2006), respectively. Since these objects have measured masses of $96 \pm 9 M_J$ (OGLE-TR-122b) and $89 \pm 12 M_J$ (OGLE-TR-123b), the plots are for a mass range from 60 to 120 M_J . The measured radii are $1.17^{+0.23}_{-0.13} R_J$ and $1.30 \pm 0.11 R_J$ for OGLE-TR-122b and OGLE-TR-123b, respectively, and the plotted radius range is 0.8 to 1.6 R_J . See text for a discussion of the issues involved.